Endotoxemia increases the clearance of mPEGylated 5000-MW quantum dots as revealed by multiphoton microvascular imaging

Ryon M. Bateman
Kevin C. Hodgson
Kapil Kohli
Darryl Knight
Keith R. Walley
University of British Columbia
Critical Care Research Laboratories
James Hogg iCAPTURE Centre
St. Paul's Hospital
Vancouver, British Colombia, Canada, V6Z 1Y6

Abstract. Imaging the microcirculation is becoming increasingly important in assessing life-threatening disease states. To address this issue in a highly light absorbing and light scattering tissue, we use laser scanning multiphoton microscopy and fluorescent 655-nm 5000-MW methoxy-PEGylated quantum dots to image the functional microcirculation deep in mouse hind limb skeletal muscle. Using this approach, we are able to minimize *in vivo* background tissue autofluorescence and visualize complete 3-D microvascular units, including feeding arterioles, capillary networks, and collecting venules to depths of 150 to 200 μm. In CD1 mice treated with lipopolysaccharide to model an endotoxemic response to bacterial infection, we find that these quantum dots accumulate at microvascular bifurcations and extravasate from the microcirculation in addition to accumulating in organs (liver, spleen, lung, and kidney). The quantum dots are cleared from the circulation with a first-order elimination rate constant seven times greater than under normal conditions, 1.6 ± 0.06 compared to 0.23 ± 0.05 h^{-1}, $P < 0.05$, thereby reducing the imaging time window. *In vitro* experiments using TNFalpha treated isolated leukocytes suggest that circulating monocytes (phagocytes) increased their nonspecific uptake of quantum dots when activated. In combination with multiphoton microscopy, quantum dots provide excellent *in vivo* imaging contrast of deep microvascular structures. [DOI: 10.1117/1.2822882]

Keywords: quantum dots; multiphoton microscopy; microcirculation; inflammation.

Paper 07128R received Apr. 4, 2007; revised manuscript received Jul. 20, 2007; accepted for publication Aug. 28, 2007; published online Dec. 18, 2007.

1 Introduction

High-resolution microvascular imaging has provided insights into cancer pathophysiology[1,2] and is increasingly important in the field of critical care medicine as microvascular function has been associated with survival in patients with severe bacterial infection.[3] In patients, the sublingual (tongue) microcirculation has become an important imaging target for assessing superficial microvascular geometry using orthogonal polarization spectroscopy (OPS) imaging.[3,4] Experimentally, the skeletal muscle microcirculation has been used to investigate microvascular oxygen transport in animal models of bacterial infection using intravital video microscopy.[5] While the sublingual microcirculation is convoluted, the skeletal muscle microvascular unit is well defined, consisting of three components: (1) feeding arterioles, which are resistance vessels and deliver blood to the tissue; (2) capillary networks, which distribute individual red blood cells throughout the tissue; and (3) collecting venules, which are larger capacitance microvessels that collect and return blood to the general circulation.

To achieve increased optical imaging resolution, researchers have turned to multiphoton microscopy for deep tissue imaging[6–8] and fluorescent quantum dots[9,10] (QDs), which provide more imaging detail than organic probes such as FITC-dextran.[11] This combination of technologies has been used to image microvessels in highly scattering adipose tissue,[11] extravasating tumor cells in the lung,[12] and K+ channels in plasma membranes.[13] QDs are semiconductor nanocrystals consisting of a CdSe core and a ZnS shell with a dry diameter of only a few nanometers. Unlike organic fluorophores, QDs have a broad excitation spectrum, but a narrow diameter-dependent, fluorescence emission spectrum.[9,10] Moreover, they are highly photostable, have negligible temporal fluctuations and are very bright, with two-photon cross sections two to three orders of magnitude greater than conventional fluorescent probes.[11] As such, these QD nanoparticles are particularly attractive as contrast agents for deep tissue optical imaging using nonlinear multiphoton fluorescence excitation, which requires the simultaneous absorption of two or more IR photons in a femtoliter focal volume.[7,14] To

Address all correspondence to Ryon M. Bateman, Ph.D., St. Paul's Hospital, 1081 Burrard Street, Vancouver, BC, Canada, V6Z 1Y6, Tel: 604-689-0020; Fax: 604-806-8351; E-mail: rbateman@mrl.ubc.ca

1083-3668/2007/12(6)/064005/8/$25.00 © 2007 SPIE

render QDs water soluble, however, they must be coated with amphiphilic materials. Coating nanoparticles with polyethylene glycol (PEG) serves two important purposes. First, it renders nanoparticles biologically useful as an imaging contrast agent, and second, PEGylation increases nanoparticle circulating half-life.[11,15]

In this paper, we report on the use of methoxy-PEGylated (mPEG, 5000 MW) 655-nm QDs for deep tissue *in vivo* microvascular imaging in mouse skeletal muscle using multiphoton microscopy. We show that complete microvascular units, including 4 to 5-μm-diam capillaries, can be readily identified at tissue depths of 150 to 200 μm. We confirm previous observations that QDs accumulate in various tissues, but also show that QD aggregates accumulate in particular microvascular locations and extravasate from the microcirculation. We also report that QDs are rapidly cleared during the onset of endotoxemia, thereby reducing their effective time window as an imaging contrast agent.

2 Materials and Methods

2.1 *QDs*

For this work, nontargeted methoxy-PEGylated (5000-MW) 655-nm QDs (maximum fluorescence emission 655 nm) were supplied by Quantum Dot Corporation (Hayward, California). Immediately prior to injection, QDs were sonicated for 10 min in an ice bath to break up any aggregates that might have formed and mixed 30/70 (vol/vol) with saline to a working concentration of 0.6 μM. In preliminary studies comparing the fluorescent signal from equimolar solutions of 565- and 655-nm mPEG-5000 QDs, we found the larger CdSe-ZnS core-shell nanoparticles to be the "brighter" of the two when excited at 900 nm. The larger QDs with emission maximum at 655 nm also had the advantage of being further red-shifted from the skeletal muscle tissue autofluorescence background signal.

2.2 *Animal and Extensor Digitorum Longus Muscle Preparation*

Male CD1 mice, weighing 30 to 35 grams, were anesthetized by an intraperitoneal injection of ketamine (112.5 mg/kg) and xylazine (15 mg/kg) and placed on a 37 °C heating pad. The left hind limb was shaved and surface hair removed as it interfered with fluorescent imaging. The extensor digitorum longus (EDL) skeletal muscle was blunt dissected and severed at the tendon. The animal was placed in the recovery position with its leg extended into a WillCo-glass-bottom dish (Amsterdam, The Netherlands), for imaging using an inverted microscope, and the muscle held under tension by a suture tied to the EDL tendon. The muscle was bathed in warm saline, maneuvered into the optical beam path, and covered by a piece of Saran Wrap, which acted as an oxygen permeability barrier. Then 60 pmols of QDs were injected into the circulation via the tail vein. Approximating the mouse blood volume at 2 mL, we estimated the initial QD circulating concentration to be 20 nM. The animal was then covered with a heating pad to maintain internal core temperature. To assess the effect of an endotoxemic response on QD clearance, a mouse model of bacterial infection was used where gram negative bacterial cell wall lipopolysaccharide (LPS) was mixed with saline (20 mg/kg, *Escherichia coli* 0111:B4 LPS, Sigma, Saint Louis, Missouri) and injected intraperitoneally. Since the microvascular response to LPS takes several hours to develop, QDs were injected 3.5 h after LPS injection. All procedures were approved by the Animal Care Committee at the University of British Columbia.

2.3 *Multiphoton Microscopy*

To facilitate *in vivo* microvascular imaging in the highly light absorbing and scattering skeletal muscle tissue, we used a titanium sapphire mode-locked 100-fs pulse laser (Spectra Physics, Mountain View, California), with a 80-MHz repetition rate, tuned to 900 nm and focused through a $20\times/0.7$ numerical aperture (NA) water-immersion objective (AOBS SP2 TCS laser scanning confocal microscope, Leica Microsystems, Heidelberg GmbH, Mannheim). The power out of the objective was 30 mW; however, the power at the focal plane within the muscle was unknown. Fluorescent images were acquired at 400 Hz using either single-frame acquisition or three frame averaging. Optical sectioning was performed using Nyquist sampling. In time course experiments to determine QD circulating half-life, imaging parameters were adopted on the fly to optimize the dynamic range of the initial fluorescence reading. Larger microvessels near the surface of the skeletal muscle were chosen to follow the *in vivo* QD elimination as they were the easiest vessels to find quickly following injection and provided good imaging targets of not only intravascular fluorescence, but also of local QD accumulation near microvessel bifurcations and for tracking of extravasating QD aggregates. To determine what multiphoton excitation wavelength would best minimize endogenous background autofluorescence in skeletal muscle, tissue was excited over a range of wavelengths from 730 to 900 nm and spectral emission scans with 10-nm bandwidths were collected from 450 to 625 nm.

2.4 *Analysis of In Vivo QD Elimination*

To quantify QD elimination, fluorescence intensity was measured in defined regions of interest within microvessels and the surrounding tissue and normalized to baseline. Intensity values were corrected for background, which was determined in the extravascular space surrounding the blood vessels. Visual inspection of the fluorescent time-course profiles indicated that QDs were eliminated from LPS-treated mice much more rapidly than controls. To quantify *in vivo* circulating kinetics we determined elimination rate constants (Kel) and circulating QD half-lives ($t_{1/2}$) in three control and three LPS treated mice. QD clearance was modeled as a first order elimination reaction where

$$-\mathrm{dQD/d}t = (\mathrm{Kel})(\mathrm{QD}). \tag{1}$$

Solving and rearranging Eq. (1) to the form $\ln(\mathrm{QD/QDo}) = (\mathrm{Kel})(t)$, where QD/QDo is normalized fluorescence, t is time, and Kel is the elimination rate constant, enabled us to determine Kel by linear regression and $t_{1/2}$ algebraically. A t test was performed (SigmaStat 3.0, Systat Software Inc, Richmond, California) to test for differences in Kel and circulating half-life between groups.

While we found no increase in background fluorescent signal in general, we did observe some evidence of QD

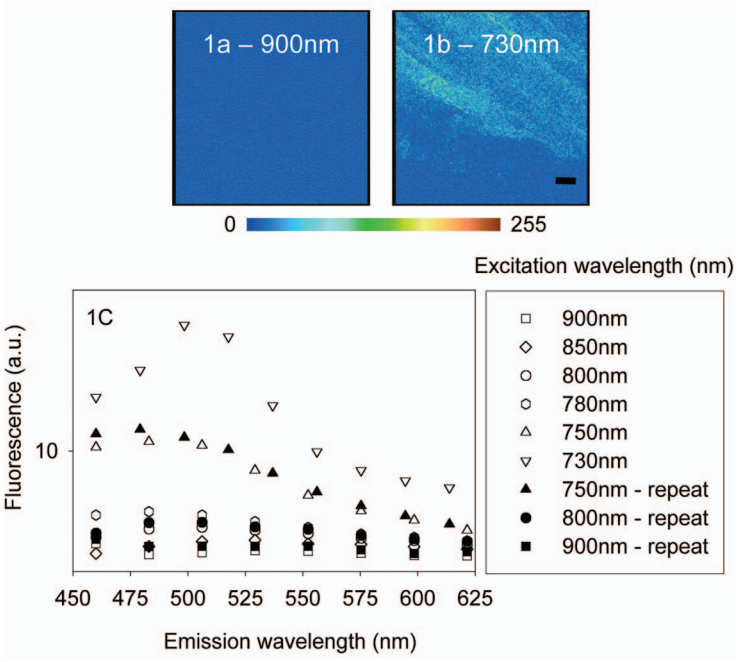

Fig. 1 Multiphoton excitation wavelength dependence of mouse hind limb skeletal muscle autofluorescence. (a) Tissue autofluorescence when excited at 900 nm compared to (b) the same tissue excited at 730 nm, 20×/0.7 NA water-immersion objective with emission bandwidth 450 to 600 nm; power was 30 mW out of the objective. (c) Spectral profiles obtained from an imaging series ranging from tissue excitation at 900 to 730 nm with 10 nm emission bandwidths. To test for possible photobleaching, images were reacquired at 750, 800, and 900 nm. The scale bar is 20 μm.

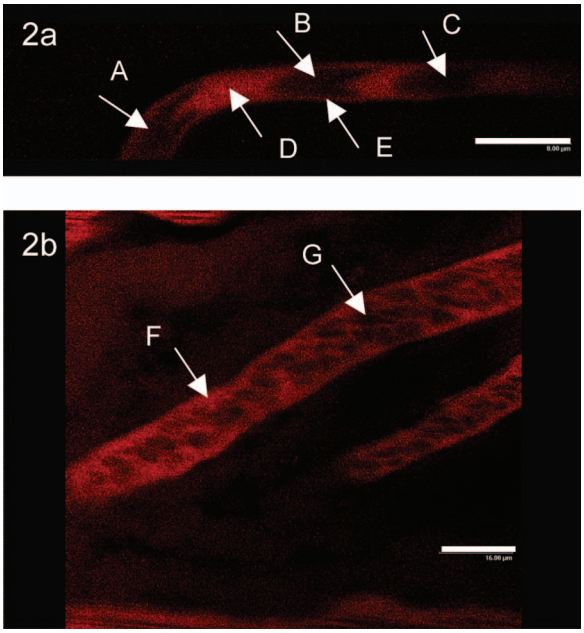

Fig. 2 Optical sections of skeletal muscle microvessels. Multiphoton rapid scans (4000 Hz) of (a) a single capillary and (b) microvascular arterioles using an upright laser scanning confocal microscope configuration show that QDs are confined to the plasma space between red blood cells (900-nm excitation, fluorescent emission 600 to 700 nm, 40×/0.8 NA dipping objective). In (a) we see a train of red blood cells flowing through a capillary; red blood cells (arrows A, B, and C) are nonfluorescent and detected by contrast with the fluorescent QDs filled plasma gaps (arrow D). The characteristic red blood cell "tail" is indicative of red blood cell deformation as it passes through a capillary diameter smaller than its own diameter. A thin fluorescent layer can be seen between the red blood cell and the capillary cell wall (arrow E). In larger diameter arterioles (b) red blood cells retain their discoid shape (arrow G). Arrow F indicates fluorescent plasma. The scale bars are 8 and 16 μm, respectively.

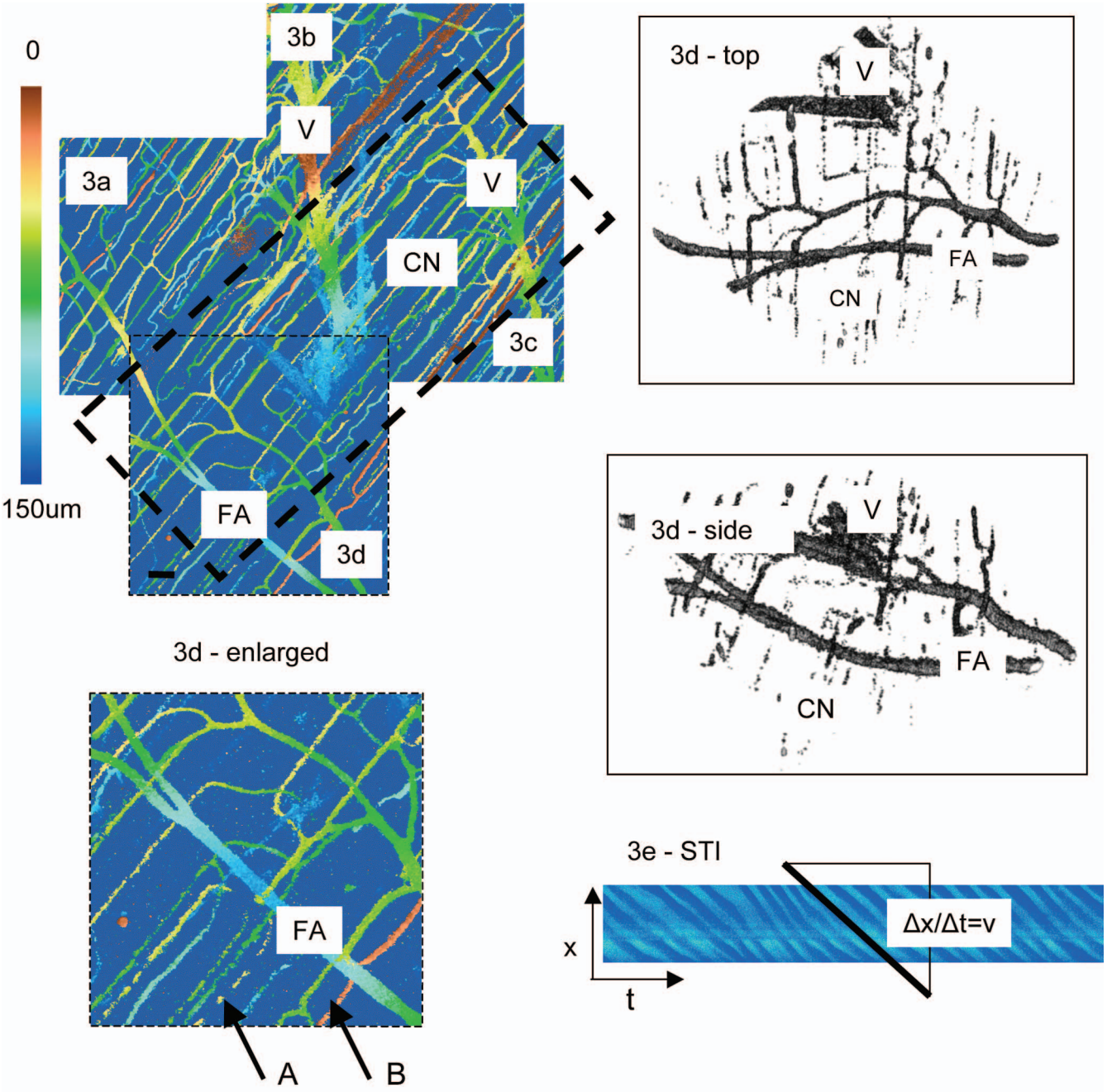

Fig. 3 *In vivo* three-frame average composite multiphoton image of the skeletal muscle microcirculation using fluorescent 655-nm QDs with emission range of 600 to 700 nm. Excitation at 900 nm was delivered through a 20×/0.7 NA water-immersion objective lens with 30 mW out of the objective. The capillary network is orientated within the dashed lines from 7 to 2 o'clock. In the centre of the image, a deep collecting venule (V) is running beneath the capillary network (CN), which is supplied by feeding arterioles (FA) on the left and drained by a collecting venule on the right. Color bar indicates depth. Scale bar is 20 μm. The enlarged panel (d) distinguishes between flowing capillaries with continuous fluorescent signal (arrow B) and stopped-flow capillaries with a punctate fluorescent signal (arrow A). Different perspectives of a single frame image from panel (d) show both fluorescent plasma gaps (dark objects, liquid phase) and nonfluorescent red blood cells (bright spaces, solid phase), indicative of the two phase nature of capillary blood flow. (e) Space time image (STI) generated from a line scan (milliseconds per line) across a single capillary, where x and t are the spatial and time dimensions, respectively. Red cell velocity can be calculated from the slope of the dark bands, while red cell lineal density can be determined from the number of red cells (dark bands) at a given time.

aggregates accumulating in and extravasating from the skeletal muscle microcirculation of LPS-treated mice. Since LPS is known to activate components of the reticuloendothelial and immune system including macrophages (liver Kupffer cells and circulating monocytes) and leukocytes that roll and adhere to the microvascular endothelium, we suspect that these cells were accumulating QDs *in vivo*. To assess whether activated leukocytes could nonspecifically accumulate QDs,

we isolated mouse leukocytes from whole blood using 7% dextran (100,000 to 200,000 kDa; Sigma, Ontario) (1/1 vol/vol). Washed leukocytes were resuspended in RPMI-1640 medium (Invitrogen, Ontario) and incubated at 37 °C/5% CO_2 for 3 h with TNFalpha (200 ng/ml) in the presence of QDs at the estimated 20 nM *in vivo* concentration used for microvascular imaging. TNFalpha is a proinflammatory mediator that activates leukocytes and macrophages. Cells were fixed using 4% paraformaldehyde and analyzed using flow cytometry (Epics XL-MCL, Beckman Coulter, Fullerton, California).

3 Results

3.1 *Near IR Excitation Reduces Background Skeletal Muscle Autofluorescence*

Tissue autofluorescence arises when a variety of intrinsic molecules including NAD(P)H, flavins, retinol, tryptophan, and its indolamine derivatives are excited by UV or near-IR light.[16] To minimize tissue autofluorescence and maximize microvessel fluorescence contrast, skeletal muscle was excited in the IR at 900 nm [Fig. 1(a) versus Fig. 1(b)]. We found that exciting the tissue at increasingly longer wavelengths, from 730 to 900 nm, resulted in a reduction in peak autofluroescent signal at 500 nm [Fig. 1(c)]. Moving to longer excitation wavelengths was also advantageous for imaging skeletal muscle because it enabled deeper tissue penetration with less photon scatter. Since the autofluorescence signal ranged from below our cutoff emission wavelength of 450 nm to approximately 600 nm, which overlapped with the emission spectrum of smaller and less "bright" nontargeted 565-nm QDs, we opted to use the brighter 655-nm QDs, which have an emission maximum at 655 nm and a relatively narrow emission bandwidth from 600 to 700 nm.

3.2 *In Vivo QD Fluorescent Contrast Imaging*

Our first question regarding *in vivo* QD behavior was how they were distributed within the blood. We found QDs to occupy the plasma space between red blood cells without being incorporated into red blood cells themselves. Figure 2 shows rapid (4000-Hz) single-frame high-resolution images of red blood cells flowing through a 4 to 5-μm-diam capillary and a relatively larger 15-μm-diam feeding arteriole. Dark nonfluorescent red blood cells can clearly be distinguished from fluorescent plasma gaps containing QDs, which provide good imaging contrast between plasma, erythrocytes, and background tissue. We found no evidence that QDs were taken up by erythrocytes over the time course of this study as erythrocytes remained nonfluorescent; however, the slight speckle on some erythrocytes seen in high-resolution images suggested that there may have been some minor adsorption to the outer membrane. A thin fluorescent film was detected between the boundary of the erythrocyte membrane and the inner microvessel wall (Fig. 2(a))].

3.3 *In Vivo Microvascular Imaging Using QDs and Multiphoton Microscopy*

Since QDs provided good microvascular imaging contrast, we next evaluated their ability to facilitate deep tissue mapping of the functional microcirculation. To do this, we used multiphoton microscopy (900-nm) optical sectioning and three-frame averaging to obtain images of the mouse skeletal muscle microcirculation to depths of 150 to 200 μm. Figures 3(a)–3(d) depict a reconstructed pseudocolored (for depth) composite image of a complete skeletal muscle microvascular unit, comprising feeding arteriole, capillary network, and collecting venule. Single-frame-reconstructed 3-D black and white images [rotated to show top and side views of Fig. 3(d)] show larger dark (fluorescent) feeding arterioles branching off to individual capillaries, which run perpendicular to the feeding arterioles and parallel to muscle fibers (not shown in the image). In individual capillaries, fluorescent plasma gaps appear as dark objects, while white spaces indicate the presence of nonfluorescent red blood cells. Accordingly, the single-frame image provides static information on capillary red cell lineal density (LD, RBC/mm capillary length) and maps the 3-D microvascular architecture; however, it does not provide any dynamic information. To obtain dynamic information from a single capillary, individual line scans can be performed to generate space-time images[5,17] (STIs), which provide hemodynamic information on red cell velocity and lineal density. An example is shown in Fig. 3(e).

In contrast to the single-frame image, acquiring microvascular images using three-frame averaging (images were acquired at 400 Hz using bidirectional scan mode with off-line phase correction) identifies putative functional or flowing capillaries as the temporal and spatial variation in fluorescent plasma gaps results in a continuous fluorescent signal along the length of the capillary. Note that stopped-flow vessels, which increase in various disease states, generate a discontinuous or punctate fluorescent signal when acquired as a three-frame average because stationary nonfluorescent red blood cells produce nonfluorescent gaps in the fluorescent signal. By comparison, vessels with only plasma flow produce a continuous fluorescent signal; however, these vessels can not be deemed "functional" since they do not contain erythrocytes. In the panel in Fig. 3(d), enlarged, we see evidence of both continuous-flow (continuous fluorescent signal along the capillary) and stopped-flow capillaries (discontinuous fluorescent signal along the capillary). To determine microvascular functionality, one must assess the three-frame average image relative to the single-frame image. Comparing the nature of the fluorescent signals in three-frame and single-frame images [Fig. 3(d)], we determined that most microvessels were in fact functional, that is they showed both a continuous fluorescent signal and the presence of red blood cells.

3.4 *In Vivo QD Stability for Microvascular Imaging*

During our initial imaging studies of the inflamed microcirculation, we were surprised to find an absence of QD fluorescent signal 5 h after LPS injection. To investigate the disappearance of QDs from the circulation, we performed *in vivo* kinetic experiments by sampling the fluorescent signal in single microvessels (20 to 30-μm diameter) over time. Figure 4 shows the time course of mPEGylated (5000-MW) QD 655-nm clearance from the circulation. We found the elimination rate constant (Kel) to be almost 7 times greater in the LPS treated mice compared to control (1.6 ± 0.06 h^{-1} in LPS versus 0.23 ± 0.05 h^{-1} in control, $P < 0.05$). The increased Kel in LPS treated mice was reflected by a significant de-

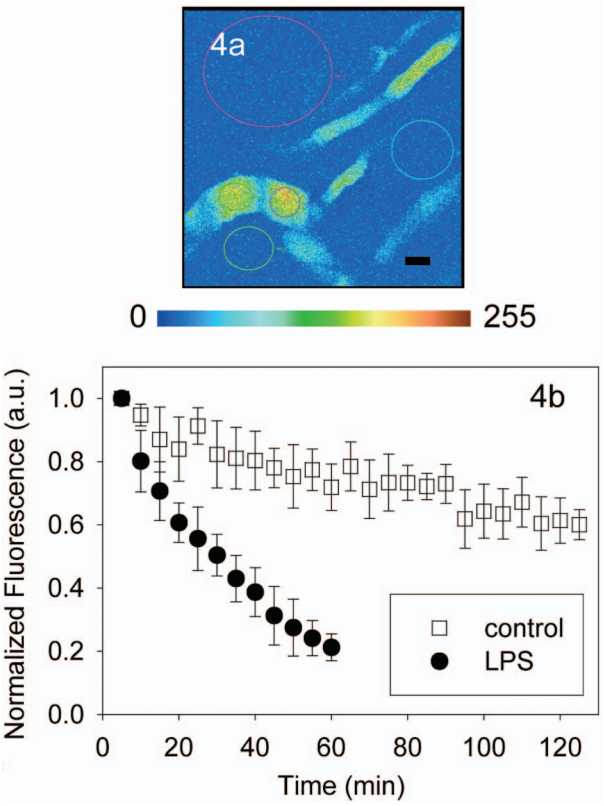

Fig. 4 QD clearance from mouse circulation: (a) example of surface skeletal muscle microvessels used to follow the *in vivo* time course of QD clearance form the circulation. Microvessels were imaged using multiphoton microscopy (900-nm excitation, 63×/1.2 NA water-immersion objective, 600 to 700-nm emission fluorescence). Circles indicate regions of interest for intravascular fluorescence and background measurements. (b) The time course of QD elimination for control and LPS treated mice. The scale bar is 20 μm.

crease in circulating QD half-life compared to control (27±2 min in LPS versus 185±36 min in control, $P<0.05$). Since the normalized QD signal in inflamed mice decreased to less than 10% by 90 min, the rapid clearance of QDs offers an explanation for why no fluorescent signal was detected by 5 h.

Table 1 Percent of isolated leukocytes that accumulate QDs.

Cell population	–TNFα (%)	+TNFα (%)
Granulocytes	79.5	84
Monocytes	71	83
Lymphocytes	50.8	47

Isolated leukocytes from CD1 mice were treated with TNFα (200 ng/ml) and incubated with quantum dots for three hours at 37°C/5% CO_2 using gentle mixing. Cells were fixed in 4% paraformaldehyde and QD fluorescence detected by flow cytometry. Values indicate the % of cells with QD signal and are the average of two samples.

While we confirmed *ex vivo* that QDs accumulate in a number of tissues including the liver, spleen, kidney, and lung (Fig. 5), we also observed the *in vivo* accumulation of QD aggregates at microvascular bifurcations in skeletal muscle (Fig. 6). Additionally, we observed the extravasation of QD aggregates from the microcirculation (Fig. 6). To assess whether activated leukocytes might enhance nonspecific QD uptake and accumulation, we isolated white blood cells and treated them with TNFalpha in the presence of QDs. Flow cytometry analysis revealed that activated monocytes (circulating phagocytes) were more likely to take up QDs than non-activated monocytes (Table 1).

4 Discussion

In this paper, we have shown that near-IR multiphoton imaging of nontargeted mPEGylated 5000-MW 655-nm QDs provides excellent *in vivo* fluorescent contrast for high-resolution imaging of the skeletal muscle microcirculation. Using this approach, we were able to minimize tissue autofluorescence and resolve all major components of the complete microvascular unit, including feeding arterioles, capillary networks, and collecting venules. This is a distinct advantage over other optical imaging modalities, bright-field microscopy, or OPS imaging, as they lack the resolving power to detect deep microvascular structures. Despite the multiphoton imaging advantage of limiting fluorescent excitation to the focal volume and nowhere else, the potential for local tissue damage re-

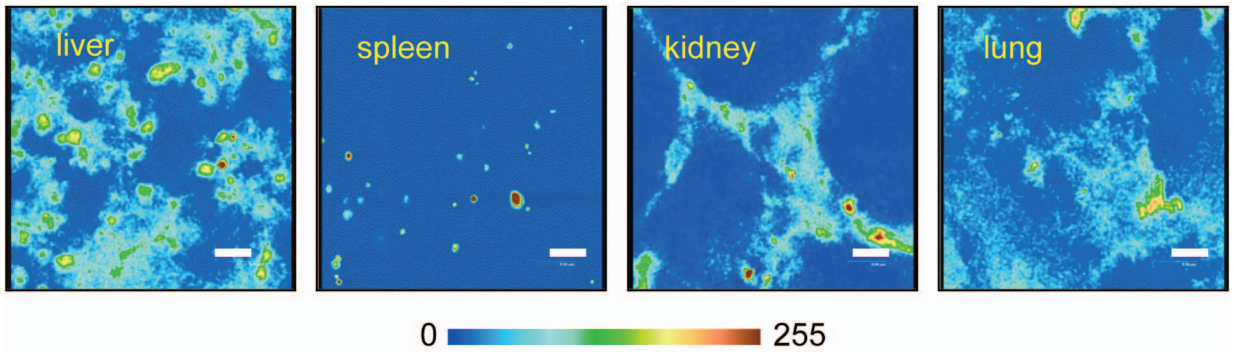

Fig. 5 Accumulation of QDs in mouse liver, lung, spleen, and kidney 5 h after treatment with LPS. Organs were removed and imaged in cross section using high-resolution multiphoton imaging (900-nm excitation, 63×/1.2 NA water-immersion objective, 600 to 700-nm emission fluorescence). While QD fluorescence was virtually eliminated from the circulation, we found evidence of QD accumulation in all organs examined. The color bar indicates fluorescent intensity and the Scale bar is 8 μm.

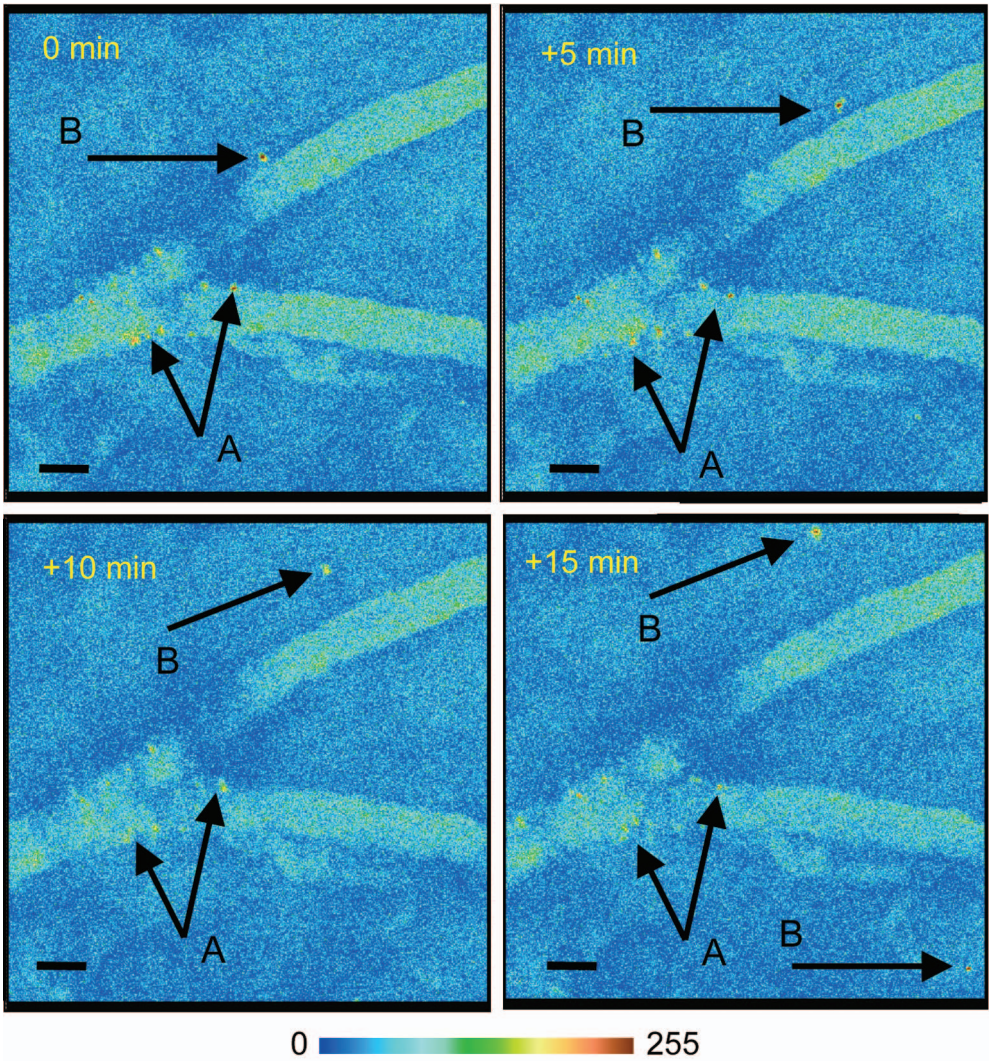

Fig. 6 QD accumulation at a microvascular bifurcation and extravasation from the skeletal muscle microcirculation in LPS-treated mice. QDs were imaged using multiphoton microscopy (900-nm excitation, 63×/1.2 NA water-immersion objective, 600 to 700-nm emission fluorescence). QD aggregates can be seen to accumulate at multiple locations near the microvascular bifurcation (arrow A) and extravasate from the microcirculation (arrow B). The color bar indicates fluorescence intensity and the scale bar is 20 μm.

mains. Working with laser powers out of the objective in the 30 to 50-mW range, we found no evidence of skeletal muscle damage or abnormal microvascular flow. This contrasts with the sensitivity of the mouse eye, where we observed that powers above a few milliwatts induced hyperemia.[18]

While we confirmed that QDs are taken up by the liver and spleen,[15,19] we also observed that mPEGylated 5000-MW QDs aggregated at microvascular bifurcations, suggesting that hemodynamic forces play a role in the biodistribution of QDs, presumably by increasing the contact time between nanoparticles and rolling or adhered leukocytes. This microvascular localization of QDs likely explains why the circulating half-life of QDs assessed by whole body noninvasive imaging was found to be twice that determined by venipuncture.[15] Using the higher imaging resolution afforded by multiphoton microscopy, we were able to avoid regions with QD accumulation and sample fluorescent signal from the center of microvessels. Not only did QD aggregates accumulate in microvascular bifurcations, but we also observed QD aggregates extravasating from the microcirculation. Here we assume that activated lymphocytes were responsible for clearing the QDs via the lymph, which may also help explain the observation that QDs accumulate in lymph nodes.[15]

An important consideration when using microvascular imaging contrast agents is their circulating half-life. While core/shell size has a negligible effect on QD clearance, increasing the length of the PEG substitution from mPEG-750 (300 residues/QD) to mPEG-5000 (100 residues/QD) increased[15] the circulating half-life 20-fold. In our study, we found that the circulating half-life of mPEG 5000-MW QDs decreased seven-fold, from 185 to 27 min, when mice were stimulated with bacterial LPS. This reduction in circulating half-life means that QD imaging should be done soon after injection to maximize image contrast between microvessels and tissue.

Since LPS causes a systemic inflammatory and coagulation response, including complement activation, increased production of acute phase proteins, and activation of macrophages, it is conceivable that an activated reticuloendothelial system,

which removes exogenous particles from the blood, was responsible for enhanced nonspecific clearance of QDs in endotoxemic mice. This is supported by our findings that QDs accumulated in endotoxemic liver, spleen, and TNFalpha-activated circulating monocytes (phagocytes). Increasing the density and length of nanoparticle surface PEGylation has been shown to reduce nonspecific uptake and increase circulating half-life in normal animals,[15,20] suggesting that additional PEGylation or other surface modifications may increase QD circulating half-life under endotoxemic conditions. Further study is required to assess the effect of extending the degree of QD PEGylation or other surface modifications on increasing the QD imaging window under endotoxemic conditions.

5 Conclusion

To translate this experimental microvascular imaging capability from the bench to the bedside will require the ability to image through the skin and deep into the highly light absorbing and scattering skeletal muscle tissue. The potential for diagnostic microvascular imaging in deep tissues looks promising as advances in technology, including femtosecond laser pulses beyond the IR range, nanocrystals with fluorescent emissions in the far-IR spectral region, increased sensitivity of photon detectors, new fiber optic systems for light delivery, and collection and optical clearing agents, will collectively enhance high-resolution optical imaging of the microcirculation in deep tissue. We believe this optical imaging approach can be extended to investigate other important microvascular phenomena in deep tissue including leukocyte behavior and microvascular permeability, which may provide better patient treatment through better diagnosis of the microvascular state.

Acknowledgments

The authors acknowledge the help of Yingjin Wang with animal experiments and Anna Merideth with flow cytometry. Support is acknowledged as follows. R. M. Bateman is a Heart and Stroke Foundation, Michael Smith Foundation for Health Research and CIHR/HSFC IMPACT Strategic Training Postdoctoral Fellow. K. R. Walley is a Michael Smith Foundation for Health Research Distinguished Scholar.

References

1. H. J. Varghese, L. T. MacKenzie, A. C. Groom, C. G. Ellis, A. F. Chambers, and I. C. MacDonald, "Mapping of the functional microcirculation in vital organs using contrast-enhanced in vivo video microscopy," *Am. J. Physiol. Heart Circ. Physiol.* **288**(1), H185–193 (2005).
2. M. Stroh, J. P. Zimmer, D. G. Duda, T. S. Levchenko, K. S. Cohen, E. B. Brown, D. T. Scadden, V. P. Torchilin, M. G. Bawendi, D. Fukumura, and R. K. Jain, "Quantum dots spectrally distinguish multiple species within the tumor milieu in vivo," *Nat. Med.* **11**(6), 678–682 (2005).
3. Y. Sakr, M. J. Dubois, D. De Backer, J. Creteur, and J. L. Vincent, "Persistent microcirculatory alterations are associated with organ failure and death in patients with septic shock," *Crit. Care Med.* **32**(9), 1825–1831 (2004).
4. P. E. Spronk, C. Ince, M. J. Gardien, K. R. Mathura, H. M. Oudemans-van Straaten, and D. F. Zandstra, "Nitroglycerin in septic shock after intravascular volume resuscitation," *Lancet* **360**(9343), 1395–1396 (2002).
5. C. G. Ellis, R. M. Bateman, M. D. Sharpe, W. J. Sibbald, and R. Gill, "Effect of a maldistribution of microvascular blood flow on capillary O(2) extraction in sepsis," *Am. J. Physiol. Heart Circ. Physiol.* **282**(1), H156–164 (2002).
6. W. Denk, J. H. Strickler, and W. W. Webb, "Two-photon laser scanning fluorescence microscopy," *Science* **248**(4951), 73–76 (1990).
7. W. R. Zipfel, R. M. Williams, and W. W. Webb, "Nonlinear magic: multiphoton microscopy in the biosciences," *Nat. Biotechnol.* **21**(11), 1369–1377 (2003).
8. P. T. So, C. Y. Dong, B. R. Masters, and K. M. Berland, "Two-photon excitation fluorescence microscopy," *Annu. Rev. Biochem.* **2**, 399–429 (2000).
9. W. C. Chan and S. Nie, "Quantum dot bioconjugates for ultrasensitive nonisotopic detection," *Science* **281**(5385), 2016–2018 (1998).
10. M. Bruchez, Jr., M. Moronne, P. Gin, S. Weiss, and A. P. Alivisatos, "Semiconductor nanocrystals as fluorescent biological labels," *Science* **281**(5385), 2013–2016 (1998).
11. D. R. Larson, W. R. Zipfel, R. M. Williams, S. W. Clark, M. P. Bruchez, F. W. Wise, and W. W. Webb, "Water-soluble quantum dots for multiphoton fluorescence imaging in vivo," *Science* **300**(5624), 1434–1436 (2003).
12. E. B. Voura, J. K. Jaiswal, H. Mattoussi, and S. M. Simon, "Tracking metastatic tumor cell extravasation with quantum dot nanocrystals and fluorescence emission-scanning microscopy," *Nat. Med.* **10**(9), 993–998 (2004).
13. V. Nechyporuk-Zloy, C. Stock, H. Schillers, H. Oberleithner, and A. Schwab, "Single plasma membrane K+ channel detection by using dual-color quantum dot labeling," *Am. J. Physiol.: Cell Physiol.* **291**(2), C266–269 (2006).
14. F. Helmchen and W. Denk, "Deep tissue two-photon microscopy," *Nat. Methods* **2**(12), 932–940 (2005).
15. B. Ballou, B. C. Lagerholm, L. A. Ernst, M. P. Bruchez, and A. S. Waggoner, "Noninvasive imaging of quantum dots in mice," *Bioconjugate Chem.* **15**(1), 79–86 (2004).
16. W. R. Zipfel, R. M. Williams, R. Christie, A. Y. Nikitin, B. T. Hyman, and W. W. Webb, "Live tissue intrinsic emission microscopy using multiphoton-excited native fluorescence and second harmonic generation," *Proc. Natl. Acad. Sci. U.S.A.* **100**(12), 7075–7080 (2003).
17. D. Kleinfeld, P. P. Mitra, F. Helmchen, and W. Denk, "Fluctuations and stimulus-induced changes in blood flow observed in individual capillaries in layers 2 through 4 of rat neocortex," *Proc. Natl. Acad. Sci. U.S.A.* **95**(26), 15741–15746 (1998).
18. R. M. Bateman, K. C. Hodgson, C. Van Breeman, and K. R. Walley, "Microvascular geometry and differential permeability in the eye during inflammation revealed with dual channel multiphoton microscopy," in *Multiphoton Microscopy in the Biomedical Sciences VI*, E. A. Periasamy and P. T. C. So, Eds., *Proc. SPIE* **6089**, 60891Y (2006).
19. M. E. Akerman, W. C. Chan, P. Laakkonen, S. N. Bhatia, and E. Ruoslahti, "Nanocrystal targeting in vivo," *Proc. Natl. Acad. Sci. U.S.A.* **99**(20), 12617–12621 (2002).
20. V. C. Mosqueira, P. Legrand, J. L. Morgat, M. Vert, E. Mysiakine, R. Gref, J. P. Devissaguet, and G. Barratt, "Biodistribution of long-circulating PEG-grafted nanocapsules in mice: effects of PEG chain length and density," *Pharm. Res.* **18**(10), 1411–1419 (2001).